

David M. Smith

# Hard X-ray and $\gamma$ -ray Detectors

Received: date

## ABSTRACT

The detection of photons above 10 keV through MeV and GeV energies is challenging due to the penetrating nature of the radiation, which can require large detector volumes, resulting in correspondingly high background. In this energy range, most detectors in space are either scintillators or solid-state detectors. The choice of detector technology depends on the energy range of interest, expected levels of signal and background, required energy and spatial resolution, particle environment on orbit, and other factors. This section covers the materials and configurations commonly used from 10 keV to  $>1$  GeV.

## 1 Introduction

Most high energy detectors in space are based on scintillators or solid-state detectors. Scintillators are the older technology and are generally used where large detector volumes and lower cost are paramount. Solid-state diode detectors, e.g. germanium, silicon, and cadmium telluride (CdTe) or cadmium zinc telluride ( $\text{Cd}_{1-x}\text{Zn}_x\text{Te}$  or CZT), generally have better energy resolution than scintillators and a lower energy threshold, and can be more easily pixellated for fine spatial resolution if that is required. They are more expensive than scintillators and more difficult to produce, package and read out in large volumes.

For all these materials, photons are detected when their energy is transferred to electrons via photoelectric absorption, Compton scattering, or pair production (which also produces positrons, of course). The high energy particles come to a stop in the detector volume, producing ionization that is detected by varying methods.

---

D. M. Smith  
Physics Department and Santa Cruz Institute for Particle Physics  
University of California, Santa Cruz, USA

I will review the most commonly used solid-state and scintillator materials and detector configurations. Considerable work has also been done worldwide on gas and liquid detectors and on newer or less common semiconductors and scintillators. For a much more detailed discussion of a wider range of detectors, as well as an excellent treatment of general considerations in photon counting and electronics, see the excellent textbook by Knoll [33].

## 2 Configurations and energy regimes

### 2.1 Thin and monolithic detectors

The optimum configuration and material for a detector depend most strongly on the energy range of the photons to be observed. Figure 1 shows the cross-sections for photoelectric absorption, Compton scattering, and pair production for photons by elements commonly used in detectors: silicon and germanium (in solid-state detectors) and iodine and bismuth (in common scintillators).

Simple efficiency calculations based on cross-sections can assist with instrument design, particularly when photoelectric interactions are dominant, but Monte Carlo simulation is the most powerful and flexible tool. It can be used to model the response to source and background radiation and to incident particles other than photons as well. The packages most commonly used are GEANT3 and GEANT4 (GEometry ANd Tracking), originally developed at the European Organization for Nuclear Research (CERN) for accelerator applications [17; 1].

Since the cross-section for photoelectric absorption is large at low energies, low-energy detectors can be quite thin. Photoelectric absorption is also a strong function of atomic number, so that, for example, a silicon detector 1 mm thick will absorb  $>50\%$  of X-rays up to 23 keV, while a 1 mm CdTe detector will do the same up to 110 keV. At these low energies, high spatial resolution is often desired when there is an imaging system using focusing optics or a coded mask (see Chapter 12). This can be accomplished with multiple small detectors, by pixellating the electrodes of solid-state detectors, or by using multiple or position-sensitive phototubes to read out a scintillator (“Anger camera” configuration, after inventor Hal Oscar Anger).

At energies of more than about 300 keV, photoelectric cross sections are small even at high atomic number, and detectors must be made large enough that photons can Compton scatter in the detector and still be photoelectrically absorbed afterwards. Even though the Compton cross section is nearly independent of atomic number, a high atomic number is still critical for stopping the downscattered photon before it escapes the detector carrying off some of its energy. A low atomic number can be desirable for the scattering plane of a Compton telescope or for a detector or shield designed to stop charged particles or X-rays and pass  $\gamma$ -rays through.

In many cases the optimum solution for maximizing sensitivity will be to have separate detectors for low energies (thin) and high energies (thick). Since most cosmic sources have falling energy spectra, high-energy detectors will generally need larger area than low-energy detectors in order to reach comparable sensitivity.

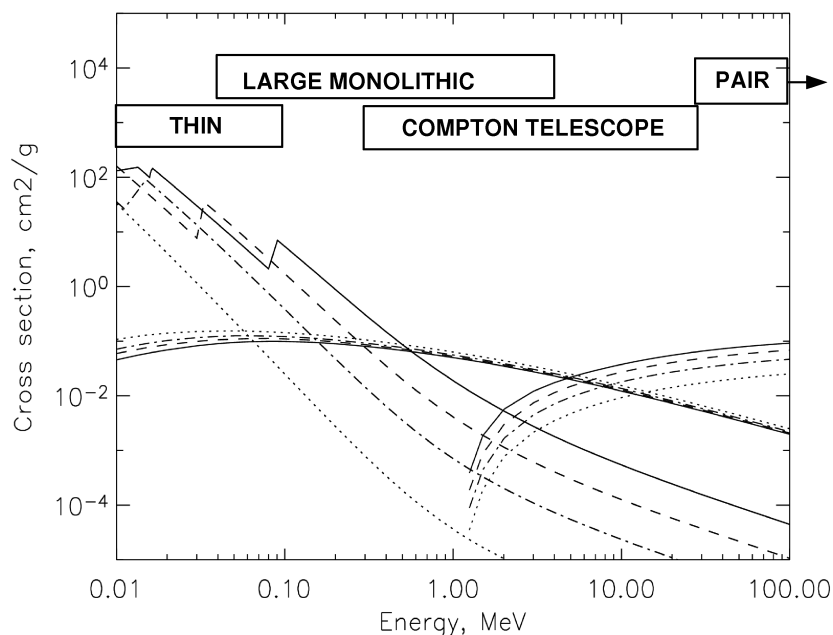


**Fig. 1** Cross-sections for photoelectric absorption (falling), pair production (rising above 1 MeV), and Compton scattering (flat). Data from Berger et al. [8]. Dotted line: silicon. Dash/dot line: germanium. Dashed line: iodine. Solid line: bismuth. The cross sections of cadmium and tellurium (i.e. CdTe and CZT detectors) are similar to iodine. The approximate energy regimes for basic detector configurations are shown (thin detectors, large monolithic detectors, Compton telescopes, and pair-tracking telescopes). The pair-tracking regime extends beyond the plot to hundreds of GeV.

Even large monolithic detectors can serve as elements for a coarse imaging system when placed in a large array. The INTERNATIONAL Gamma-Ray Astrophysics Laboratory (INTEGRAL) provides two good examples. The Spectrometer on INTEGRAL (SPI) [68] has coaxial germanium detectors with a characteristic size of 7 cm serving as pixels below a large coded mask (see Chapter 12), and the Imager on Board the INTEGRAL Spacecraft (IBIS) includes thick fingers of CsI serving as pixels beneath a finer mask than SPI's [66]. The large germanium detectors on the Reuven Ramaty High Energy Solar Spectroscopic Imager (RHESSI) [61] sit below rotation modulation collimators (see Chapter 12) that do not require position sensitivity.

## 2.2 Compton and pair tracking telescopes

At MeV and GeV energies, the physics of the photon interactions in matter can be exploited to reject background and determine the direction of the incoming photon.

In the range of a few hundred keV to tens of MeV, large-volume detectors with position sensitivity in three dimensions can record the entire sequence of Compton

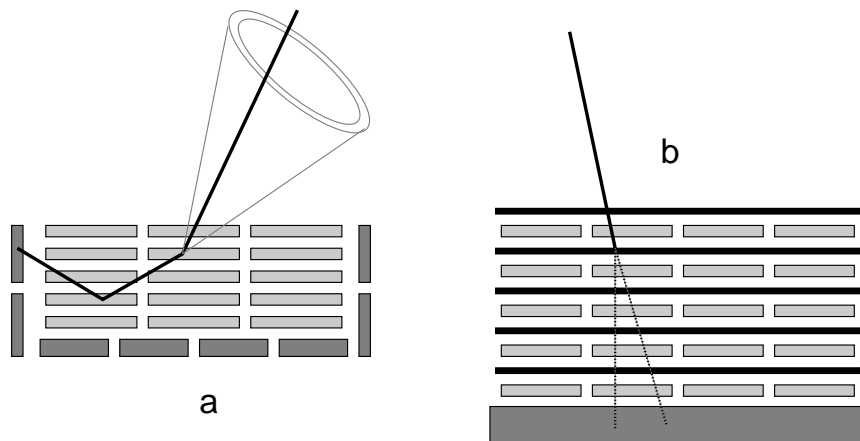


**Fig. 2** Design concepts for a modern Compton telescope (a) and pair telescope (b). The energies and angles between interactions in the Compton telescope trace the incident photon to an annulus on the sky. Here the telescope is shown with low-Z scattering detectors and high-Z absorbing detectors [11; 72; 63], although single-medium instruments are also being designed and built [13; 35; 4]. See Chapter 11 for more details. The pair telescope represents the GLAST design [6], with passive tungsten layers to convert the  $\gamma$  into an  $e^+e^-$  pair, silicon detectors to track the pair, and a heavy calorimeter to absorb the remaining energy. Relativistic beaming of the pair and high spatial resolution allows reconstruction of the incident photon's direction.

ton interactions in the detector volume. This allows the direction of the incoming photon to be reconstructed and background to be rejected effectively (see Chapter 11).

At energies of several tens of MeV and higher, where pair production is the dominant photon interaction with matter, a pair-conversion tracking system can be used. For example, the Large Area Telescope (LAT) [6] on the Fermi Gamma-ray Space Telescope consists of alternating thin layers of passive tungsten and active silicon strip detectors (Figure 2b). Pair production takes place in the tungsten, since the high atomic number gives a high cross-section (Figure 1). The electron/positron pair has high enough energy to penetrate multiple W/Si layers; the penetration depth gives the initial  $\gamma$ -ray energy, while the position-sensitive detectors allow the track to be extrapolated backwards to give the arrival direction of the  $\gamma$ -ray. The highest-energy pairs that penetrate the tracker are stopped in a calorimeter. At GeV energies, this extrapolation can be very precise. The tracking detectors are not required to measure deposited energy.

### 3 Detector materials

#### 3.1 Scintillation detectors

Scintillators can be produced in large, monolithic volumes, and in a variety of shapes. They can have low to high atomic numbers (and therefore stopping power), ranging from plastic scintillators at the low end to bismuth germanate

( $\text{Bi}_4\text{Ge}_3\text{O}_{12}$  or BGO) at the high end. Plastic scintillators can be doped with high-Z atoms, like lead, to improve their stopping power.

In inorganic scintillators, ionization produces free electrons that can move around the crystal until falling back into the valence band. In *activated* crystals, such as NaI(Tl) and CsI(Na), the trace activator element provides a fast route to the valence band via intermediate states. Since the amount of activator is small, the crystal remains transparent to the scintillation photon emitted when the activator's excited state decays. In unactivated crystals such as BGO, one ion of the pure crystal ( $\text{Bi}^{3+}$ ) provides the scintillation photons, with a large enough shift between its emission and absorption frequencies that the crystal is still transparent. In organic scintillators (plastic and liquid), large molecules are excited by the passing energetic particles; the scintillation is produced when they relax to their ground state. In all cases, scintillation light can be collected and multiplied by a sensor such as a photomultiplier tube (PMT), photodiode, or microchannel plate. Scintillation light can be reflected many times before being collected, so the PMT(s) need not have a direct line of sight to every part of the detector. In fact, uniformity of light collection – and therefore energy resolution – is sometimes improved by treating the surfaces of the best-viewed parts of the detector so that they reflect scintillation light poorly.

In space applications, extremely high energy deposits, up to many GeV, can occur in a detector due to the passage of a cosmic-ray iron nucleus (or other heavy element) or the spallation of a nucleus in the detector by any cosmic ray. NaI [22] and CsI [29] scintillators display phosphorescence in which a fraction of the light is emitted over a much longer time (hundreds of milliseconds) than the primary fluorescence. Thus, when a particularly large energy deposit occurs, the crystal can glow rather brightly for up to a second; the effect on the data depends on the design of the electronics.

Pulse shape analysis, whether by analog electronics or via flash digitization of the PMT signal, has multiple uses for scintillators. If two different scintillators have very different light decay times, they can be read out by a single phototube if they are sandwiched together, with the energy deposited in each still separable in the PMT signal. This can be used as a form of active shielding to veto charged particles or photons that interact in both scintillators. This configuration is called a “phoswich” (phosphor sandwich). Pulse shape analysis can also be used to distinguish neutron and cosmic-ray ion interactions from the interactions of photons or electrons in CsI [10] and plastic and liquid scintillators [46].

Table 1 summarizes some properties of the scintillators most commonly used in space, as well as two particularly promising lanthanum halide scintillators that have recently become available. These new materials have good stopping power and excellent energy resolution (3–4% FWHM at 662 keV versus about 7% for the industry standard NaI). They have a moderate internal radioactivity giving a count rate of  $\sim 1.8 \text{ cm}^{-3}\text{s}^{-1}$ , mostly from  $^{138}\text{La}$  [49]. This is of the same order as the background from other sources that an unshielded detector would receive in low-Earth orbit, but could dominate the background if the detector is well shielded (see section 4.1 below).

**Table 1** Properties of Some Scintillators

Material	Light Yield (photons/keV)	Decay Time (ns)	Peak $\lambda$ (nm)	Density (g/cm <sup>3</sup> )	Max. Atomic #	Notes
NaI(Tl)	38	230	415	3.67	53	1
CsI(Na)	39	460, 4180	420	4.51	55	2
CsI(Tl)	65	680, 3340	540	4.51	55	2
BGO	8.2	300	480	7.13	83	3
GSO	9.0	56, 400	440	6.71	64	4
BC-408	10.6	2.1	425	1.03	6	5
LaBr <sub>3</sub> (Ce)	63	16	380	5.29	57	6
LaCl <sub>3</sub> (Ce)	49	28	350	3.85	57	7

1 Good energy resolution. Hygroscopic; phosphorescent; Susceptible to thermal shock.

2 Slightly hygroscopic; phosphorescent. Denser, less brittle than NaI. Pulse-shape discrimination of particle types is possible.

3 Excellent stopping power; inferior energy resolution; easily machined; non-hygroscopic.

4 Gd<sub>2</sub>SiO<sub>5</sub>; non-hygroscopic. Used in the Hard X-ray Detector (HXD) on Suzaku [64]. 5 A commonly used plastic.

6 New material; some internal background from radioactivity. Best energy resolution, good stopping power.

7 Similar to LaBr<sub>3</sub>, resolution and density not quite as high. Large crystals were developed earlier.

Data are taken from Tables 8.1 and 8.3 of Knoll [33] and from Bicron [9].

### 3.2 Semiconductor detectors

In semiconductor detectors, the electrons and holes excited into the conduction band by the passage of energetic particles are swept toward opposite electrodes on the detector surface by an applied electric field. The image charges induced on one or both electrodes, as they change with the movement of electrons and holes in the crystal, provide a small current pulse. This pulse is generally read by a charge-sensitive (integrating) preamplifier, followed by a shaping amplifier.

Semiconductor detectors are capable of much better energy resolution than scintillators, since the collection of electrons in the conduction band is much more complete than the conversion to scintillation light and light collection in scintillators. The noise performance of the electronics must be excellent, however, if the natural resolution of the detector is to be approached – i.e., the limit due to counting statistics of the electron/hole pairs liberated (including the Fano factor [33, page 366]). In the preamplifier, noise currents are converted to voltage noise proportional to the detector capacitance [62, page 33]; thus detectors with large volume can be expected to show poorer resolution. Resolution can be preserved at large volumes if the electrode configuration has intrinsically low capacitance. Examples of such configurations are silicon drift detectors [54] and germanium LO-AX<sup>TM</sup> [50] and drift [42] detectors, which have one large and one small, more pointlike electrode. Pixellating the anode and reading out each pixel as a separate detector also results in low capacitance and excellent noise performance. Some of the most common semiconductor detector and electrode configurations are sketched in Figure 3.

Large energy deposits from cosmic rays in semiconductor detectors do not carry the risk of long-duration detector response that they do in scintillators. It is very important, however, to test the response of the *electronics* to huge energy

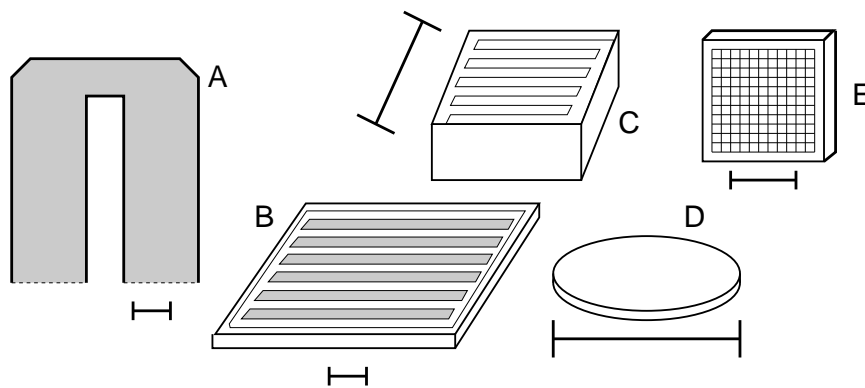


**Fig. 3** Common electrode configurations for solid state detectors. Each is shown with a 1 cm marker to indicate the scale of a typical detector. A) Coaxial germanium detector (cross section of a cylindrically symmetrical shape). Electrodes are on the inner bore and the outer surface; the insulating surface is at the back (dashed line). B) Silicon strip detector (typically  $300\ \mu\text{m}$  thick, 1 mm strips). C) Monolithic CZT detector with coplanar (interleaved) electrode to null the signal from the holes and improve energy resolution [43]. D) Simple silicon p-i-n diode with plane electrodes at top and bottom. E) CZT pixel detector. The pixel and strip detectors are shown with guard rings around the edge, used to capture any leakage current on the side surfaces and keep it away from the electronics chains reading out the volume of the detector. Pixel and strip detectors have been made from all the common semiconductor materials (Ge, Si, CZT/CdTe).

deposits. Many designs can become paralyzed for a significant amount of time by a multi-GeV energy deposit, or else produce false counts by triggering on ringing. Interactions this energetic do not occur in the laboratory, where the only cosmic ray particles are muons, so they ought to be simulated either at an accelerator or with a pulser before any electronics design is declared ready for space flight.

An extensive treatment of semiconductor detectors and their electronics is given by Spieler [62].

### 3.2.1 Germanium

Germanium detectors are preminent for spectroscopy in the range from hundreds of keV to a few MeV. Germanium crystals can be grown in large volumes at extremely high purity, with single detectors up to 4 kg [57]. High purity guarantees that both electrons and holes can move untrapped through the whole crystal volume, and that the detector volume can be depleted of charge carriers due to impurities by a manageable applied field of  $\sim 500\text{--}1000\ \text{V/cm}$ . The small bandgap gives good counting statistics for the liberated electron/hole pairs, but requires low operating temperatures – below 130 K, and preferably much lower – to prevent thermal excitation into the conduction band and a large leakage current [33, pg. 414].

Energy resolution of  $\sim 0.3\%$  FWHM at 662 keV can be achieved with a good detector and optimized electronics; this compares to a corresponding value of  $\sim 7\%$  for NaI(Tl) and  $\sim 3\text{--}4\%$  for the new lanthanum halide scintillators. Only if this high resolution is scientifically important should germanium be considered.

But high resolution should be considered important any time narrow lines are being observed, even if the exact profile of the line to be observed is *not* needed, and even if it is *not* necessary to separate nearby lines. Since  $\gamma$ -ray observations in space are often dominated by background, a good energy resolution reduces the amount of background against which the signal of a narrow  $\gamma$ -ray line is to be detected, greatly increasing sensitivity.

Operation of germanium detectors in space is challenging due to the need to keep them cold. Passive cooling is possible if a large area and solid angle of radiator can always be presented to deep space (avoiding the Sun, and, in low-Earth orbit, the Earth as well). This technique was used for the Transient Gamma-Ray Spectrometer (TGRS) on the Wind spacecraft [59] and the Gamma-Ray Spectrometer on Mars Odyssey [15]. Cryogenics can also be used, but they have a large mass and limited life; the germanium spectrometer on HEAO-3 ran out of cryogen after a pioneering 154-day mission [44]. Some recent instruments have relied on Stirling-cycle mechanical coolers [68; 61; 24]. The design of the radiator for waste heat is still critical in that case, but the requirements are not as severe as for passive cooling. RHESSI, for example, often has the Earth nearly filling the field of view of its radiator for part of its orbit. Cryocoolers can be very expensive to qualify for space flight and this should not be underestimated in mission planning.

All the germanium detectors mentioned above were in the closed-end coaxial configuration (Figure 3a), with an outer contact on the sides and across the front face of the detector, an inner contact lining a bore that goes most of the way through the crystal, and an intrinsic (insulating) surface on the back face. This configuration is a compromise between large volume, low capacitance (compared to two flat electrodes on either side of a comparable crystal) and the lowest possible distance between the electrodes (to keep the depletion voltage manageable). Thick germanium strip detectors are also being developed for Compton telescopes and other applications that require position sensitivity, and have already flown on the Nuclear Compton Telescope balloon payload [13]. The x and y positions are measured by localizing the charge collection to individual strips on each electrode (the strips on one side run perpendicular to those on the other), while the z position is measured by the relative arrival times of the electrons and holes at their respective electrodes [3].

In addition to cooling, the other particular challenge for germanium detectors in space is radiation damage. Defects in the crystal lattice caused by nuclear interactions of protons and neutrons create sites that can trap holes as they drift through the crystal. Electrons in the conduction band are not comparably affected. Since germanium detectors are designed to use both the electron and hole signals, hole trapping reduces energy resolution. Because protons lose energy rapidly by ionization, they must have high energy to penetrate the layers of passive material around the detector (e.g. the cryostat) and penetrate beyond the outer surface of the crystal. Depending on the detector or cryostat configuration, the lower limit on relevant proton energy is on the order of 100 MeV. Neutrons, on the other hand, can penetrate the full volume of the crystal regardless of their energy, and are relevant even at a few MeV [40]. Protons below 100 MeV can convert to neutrons via spallation in spacecraft materials and therefore still cause damage.

Strategies to reduce the effect of radiation damage include choice of orbit, operating procedures, detector geometry, shielding, and annealing.

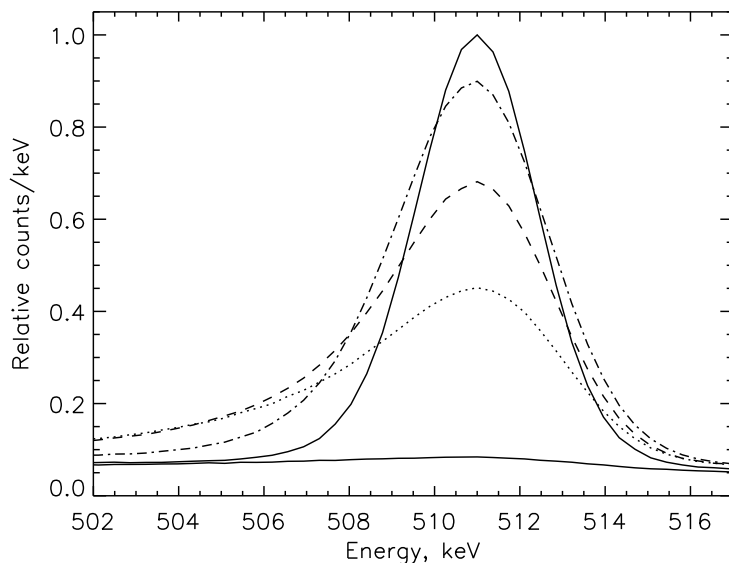


**Fig. 4** Effect of radiation damage on  $\gamma$ -ray spectroscopic performance of a coaxial germanium detector. The 511 keV background line from positron annihilation is shown in data from the RHESSI satellite taken from 2002 to 2007. The symmetrical, narrow peak is from the start of the mission. The next two lines (dot-dash and dashed) show the effect of moderate to severe damage on the line resolution due to hole trapping. The last two lines (dotted and the nearly flat solid line at the bottom) show the loss of effective area at very severe levels of damage due to volumes in the crystal that are no longer depleted (active). At this point, the RHESSI detectors were annealed. In general, an anneal would be performed at a much earlier stage of damage.

In low-Earth orbit, most radiation damage will come from radiation belt protons seen during passage through the South Atlantic Anomaly (SAA). This can be avoided if the orbit is equatorial (inclination less than about  $10^\circ$ ). This is the most benign orbit available, since the magnetosphere also protects the instrument from solar energetic particles and a large fraction of Galactic cosmic rays. In high-Earth orbit or interplanetary space, damage from Galactic cosmic rays usually dominates [34], unless a large solar energetic particle event occurs, in which case a large amount of damage can be inflicted in a short time [52; 49]. An orbit that spends much of its time in the heart of the radiation belts has by far the highest dose of all, and would certainly prohibit the use of germanium. The Space Environment Information System (SPENVIS) webpage [27] is an extremely valuable resource for estimating the irradiation by radiation-belt and solar protons in various orbits.

A good choice of detector geometry can limit the severity of the effect of radiation damage by limiting the amount of germanium that the holes must traverse. In the coaxial configuration, most of the volume is near the outside of the detector. Thus, by applying negative high voltage (HV) to the outer contact, the holes are made to take the shorter path for the majority of interactions [51]. The result is a line shape with a sharp peak and a long tail (due to the few interactions near the bore). This is shown in Figure 4. This polarity provides good uniformity of field

within the crystal for slightly n-type material. The opposite polarity (used with p-type material) will show broadening of the line much earlier and more severely as the holes migrate all the way to the central bore.

Shielding the detectors can be very effective at blocking solar and radiation-belt (SAA) protons, but not cosmic rays, which are much more energetic and penetrating. Very often, shielding is also desired to reduce background (see section 4.1 below).

Keeping the detectors very cold reduces the amount of trapping for a given radiation dose as long as the detector is never warmed up [16]. Raising the HV on a damaged detector, when possible, can reduce the effect of damage somewhat [34]. If large currents are passed through a damaged crystal, many of the hole traps will fill, and the effect of radiation damage will be much less severe for a few minutes, until these traps empty again. This occurs when a spacecraft passes through the SAA. The opposite effect occurs for damaged n-type germanium detectors when the HV is turned off: when it is turned back on, there are temporarily *more* unfilled traps than in equilibrium, and the resolution will be degraded until an equilibrium between detrapping and hole production is reached on the same timescale of minutes [32].

Even if all these factors are taken into account in design, virtually any germanium detector that is *not* in a low-Earth, equatorial orbit will have to be annealed. When the crystal is heated to well above operating temperatures, many of the damage sites become de-activated (not repaired, since the anneal temperatures are far too low to actually move atoms around in the lattice). The mechanism is not well understood. The literature includes many small-scale experiments that don't give a good, overall formula for estimating the efficacy of the anneal process given detector type, damage history, and anneal temperature and duration. Temperatures of 50° to 100 °C and durations of days to weeks are typical of operations in space [41; 15]; when in doubt, the longer and warmer, the better [16]. Some annealing does take place at room temperature [53] but takes longer to be effective, and cannot eliminate trapping completely.

### 3.2.2 Silicon

Silicon can be grown in large volumes but not to as high a purity as germanium, and is therefore harder to deplete. Silicon detectors are therefore generally thin (typically 300  $\mu\text{m}$ ), and used for purposes where that is appropriate. The thickest silicon detectors (up to  $\sim 1$  cm) are made from slightly p-type material and have lithium ions drifted through the crystal bulk to compensate the intrinsic impurities, a technique formerly used for germanium before high-purity material became available.

Small, simple planar p-i-n detectors are often used for X-ray detection up to a few 10s of keV, as in the top detector layer of the hard X-ray instrument on the Suzaku spacecraft [64]. Small Si drift detectors (SDDs), in which the field is shaped to lead the electrons to a small collecting contact, show improved resolution over p-i-n detectors due to their smaller capacitance [54] and can also provide position sensitivity when the drift time is measured in the electronics.

Large, thin Si strip detectors (single or double sided) can be used when position resolution is important but energy resolution and low energy threshold are not,

such as in the silicon tracker on the Fermi Gamma-ray Space Telescope, where the requirement is to register the passage of high-energy electrons. Thick Si strip detectors have been proposed for a Compton telescope operating in a mode where a final photoelectric absorption is not necessary [35].

Si detectors benefit from cooling to reduce leakage current, but at a more modest level than germanium (temperatures of  $-20^{\circ}$  to  $0^{\circ}\text{C}$ ). This can be accomplished by a careful passive cooling design or the use of simple thermoelectric (Peltier) coolers.

### 3.2.3 Cadmium Telluride and Cadmium Zinc Telluride

Cadmium telluride (CdTe) and cadmium zinc telluride ( $\text{Cd}_{1-x}\text{Zn}_x\text{Te}$ ) offer two advantages relative to germanium: they can be operated at room temperature and they have better photoelectric stopping power. It is difficult to grow large crystals of high quality, and the largest detectors available are  $1\text{--}4\text{ cm}^3$  [18]. Efficient detection in the MeV range therefore requires a three-dimensional array of detectors [47] to take the place of a single large germanium coaxial detector, with very careful control of passive material within the detector volume to prevent undetected Compton scatters.

When energy response greater than 30 keV is needed but it is not necessary to go above a few hundred keV, a single layer of CZT/CdTe detectors is often the best choice. If pixels of a few mm or larger are desired, an array can be made out of individual detectors, as was done for the Burst Alert Telescope (BAT) [7] on the Swift mission (CZT) and the front detector layer of the IBIS imager on INTEGRAL (CdTe) [37]. For smaller pixels, it can be advantageous to pixellate the electrode on one side of a larger detector and read signals out of each pixel. Not only does this provide greater position resolution with smaller gaps, the small pixels have very low capacitance and excellent energy resolution. Pixellated CZT detectors have been used on two hard X-ray focusing balloon payloads: the High Energy Focusing Telescope (HEFT) [14] and the International Focusing Optics Collaboration for  $\mu\text{Crab}$  Sensitivity (InFOCUS) [65]. For InFOCUS, signal traces were routed away from the detector to the ASIC electronics, while for HEFT the preamplifiers were put onto the ASIC with the same spacing as the detector pixels and bump-bonded directly to the detector. The HEFT detector technology is being adapted for the Nuclear Spectroscopic Telescope ARray (NuSTAR), an upcoming NASA Small Explorer satellite using focusing optics [25].

CZT and CdTe (and other compound semiconductors) differ from germanium and silicon in that holes are much less mobile than electrons, and suffer trapping even in crystals that are not radiation-damaged. Thus the best energy resolution is obtained when only the electrons contribute to the energy signal. This is not possible for a simple planar configuration (a rectangular detector with plane electrodes on opposite sides), but there are a number of ways to improve the situation. Coplanar grid [43; 2] and pseudo-Frisch grid [45] electrode configurations can cancel most of the contribution of the holes to the signal for thick (1 or 2 cm) single detectors, resulting in an electron-only signal that recovers the excellent energy resolution of a very thin detector. If a pixellated detector is desired for spatial resolution or low capacitance anyway, pixellating the anode also ensures that the electrons contribute most of the detected signal as they get very near the anode

(the “small pixel effect”). For a thick CZT or Cd/Te detector, it is also possible to measure the depth of the interaction within the crystal by measuring the risetime of the current pulse and use this information to correct the energy measurement either by analog or digital techniques downstream [55]. This technique was used for INTEGRAL/IBIS [37].

## 4 General Considerations

### 4.1 Background

Since most  $\gamma$ -ray detectors in space are not detecting focused radiation, count rates are often dominated by background rather than signal. Bright transient events such as cosmic  $\gamma$ -ray bursts, solar flares, and terrestrial  $\gamma$ -ray flashes are often source-dominated, but for most applications both *reducing* and *estimating* background levels is important.

For an unshielded detector in low-Earth orbit, the dominant sources of continuum background are the cosmic diffuse radiation (below about 150 keV) and the “albedo” glow of  $\gamma$ s from the Earth’s atmosphere due to interactions of cosmic rays (above 150 keV) [20; 23]. From a few hundred keV to a few MeV, radioactivity in detectors themselves and, to a lesser extent, in passive materials nearby can be a significant source of both line and continuum background. Radioactivity can be natural (e.g. from  $^{40}\text{K}$  and the daughters of  $^{238}\text{U}$ ), or induced by cosmic rays, solar or radiation-belt protons, or neutrons created in the spacecraft or in the Earth’s atmosphere. Induced radioactivity can be prompt when short-lived nuclear states have been excited, or have a half-life from seconds to years. Above a few MeV, the dominant component is likely to be from minimum-ionizing cosmic rays clipping the corners of the detector. Recently, there has been a great deal of effort put into refining tools for simulating the expected backgrounds [20; 69] (see Figure 5).

*Reducing* background should first be approached by selecting the right detector thickness (no thicker than necessary) and material (one that is not intrinsically radioactive and does not become badly so when exposed to cosmic rays on orbit). But if the instrument is not meant to observe the entire sky, there should usually also be some shielding. Below  $\sim 100$  keV, passive shielding can be adequate. It is often arranged in a “graded” configuration, with a high- $Z$  material like lead or tungsten on the outside followed by one or two layers of lower- $Z$  material, each of which is meant to stop K-shell X-rays from the previous layer before they reach the detector.

At Compton-dominated energies (see Figure 1), thick passive material would be necessary to stop incoming  $\gamma$ s. In space, however, such a shield can actually create more background than it stops, due to reprocessing of incident cosmic rays into neutrons,  $\gamma$ s, and multiple charged particles. Thus graded- $Z$  and other passive shields shouldn’t be more than a few millimeters thick. However, *active* shielding with several centimeters of inorganic scintillator can be very effective. In this case, cosmic rays are vetoed along with their daughter particles produced in the shield, and only a single interaction is necessary to veto a background photon, even if it then interacts in the central detector. An active shield will also veto photons from the target that interact in the central detector but scatter out of it (“Compton

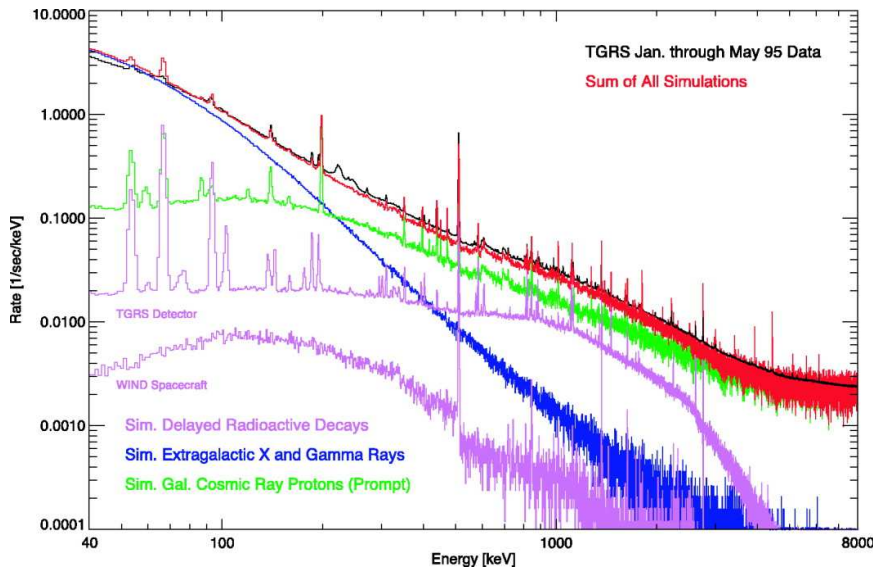


**Fig. 5** State-of-the-art *a priori* modeling of  $\gamma$ -ray instrumental background: data from Wind/TGRS and a simulation of all important background components using MGGPOD. From Weidenspointner et al. [69].

shield” mode). Even active shields produce background via neutron production [48]. A study for INTEGRAL/SPI found that 5 cm of BGO was the optimum shield thickness for its orbit [21].

At the highest energies, a thin, active plastic shield can veto the prompt components due to cosmic rays: clipping of the detector by the cosmic rays themselves and prompt nuclear de-excitations in passive materials near the detectors. But it should be established that these background components will be important in the energy range of interest before choosing to use a plastic veto. The ability to veto charged particles that are *not* cosmic rays is desirable for an orbit outside the Earth’s magnetosphere (for solar particles) or a low-Earth orbit that goes to high magnetic latitudes (for precipitating outer-belt electrons and, for nearly polar orbits, solar particles as well).

*Estimating* background is less important for detectors in imaging configurations (e.g. coded mask, rotating grid, or Compton telescope) that have ways to reject background based on incident direction. In these cases, it is enough to predict the background accurately enough to have confidence in the instrument’s sensitivity. But for non-imaging detectors, it may be necessary to know the background to 1% or better to study faint sources. This cannot be done via *a priori* modeling, if only because cosmic ray fluxes fluctuate much more than this. Instead, background is subtracted by finding a period of time when the source is not visible but the background is expected to match that during the observation. For highly collimated instruments, this is best accomplished by “chopping” between the source position and an empty field nearby, as was done with the Oriented Scintillation Spectrometer Experiment (OSSE) on CGRO and the High-Energy X-ray Timing Experiment (HEXTE) on RXTE [31; 56]. For uncollimated or wide-field instru-

ments viewing a transient event like a cosmic  $\gamma$ -ray burst or a solar flare, time intervals just before and after the event, or (in low-Earth orbit)  $\pm 15$  orbits ( $\sim$  one day) away often provide an excellent background measurement. The case of a non-chopping instrument measuring a non-transient source is the most difficult. A variety of techniques can be mixed, combining observations and modeling, including the use of the Earth as an occulter and the generation of background databases incorporating large amounts of data from throughout the mission. Such a database can be used to extract the dependence of background on parameters such as orbital position and cosmic ray flux [30; 60].

#### 4.2 Livetime

Instrumental livetime is generally of concern only when background is not – i.e. when very bright cosmic, solar or terrestrial transients are of primary interest. In these cases, all stages of the signal chain should be analyzed to make sure that the highest expected count rate can be recorded. The intrinsic response time of the detector material (scintillation light decay or electron and hole drift times in a solid state detector) may be a consideration in detector choice, but only if pulse shaping times and throughput in the rest of the electronics can be designed to keep up with the detector’s capability. Large detectors can be pixellated or replaced with many small ones to reduce deadtime, at the expense of an increase in the number of electronics chains needed. The deadtime caused by an active shield veto should always be estimated, particularly when the instrument is very large or will be studying bright transients. When scattering between detector elements is part of the source detection (such as in a Compton telescope or  $\gamma$  polarimeter), the frequency with which two independent background or source interactions will fall within the instrument’s coincidence time window by chance and be mistaken for a scatter should always be calculated.

#### 4.3 Spectral Response

Lastly, it is important to understand the energy response of any detector design due to the physics of the high-energy photon interactions. Incomplete collection of the incident photon energy is important for both line and continuum spectroscopy, but is most obvious to the eye when a narrow line is being observed. At energies where Compton scattering becomes important, a Compton continuum below the incident energy appears in the spectrum due to scattering either into or out of the detector. At low energies (within a factor of  $\sim 2$  the K-edge of the detector material), a K-shell X-ray escape peak appears since absorption occurs very close to the surface. At MeV energies, two escape peaks appear corresponding to the escape of one or both 511 keV photons following pair production and annihilation of the positron. Figure 6 shows the photopeak line, Compton backscatter feature, and first 511 keV escape peak from a RHESSI observation of the 2.223 MeV line from a solar flare, from neutron capture by a proton producing deuterium.

These effects – combined with the blurring effect of finite energy resolution – combine to make up the “response matrix”, the function that maps the input spectrum of incoming photons to the output spectrum of detector counts. Good

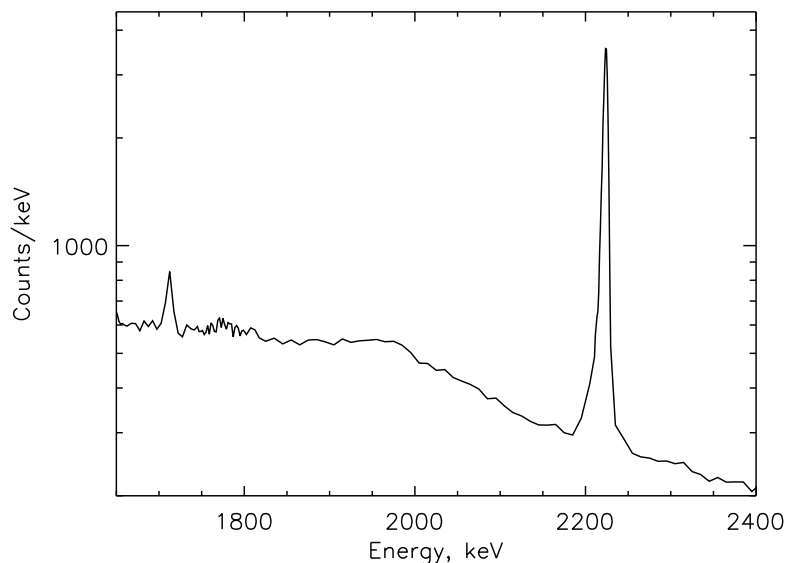


**Fig. 6** RHESSI spectrum of the solar flare of 28 October, 2003. The emission in this energy range is dominated by the response to the 2.223 MeV line, which includes the photopeak, the Compton continuum from photons that scatter nearly  $180^\circ$  out of the detector (cutting off around 2000 keV), and the first 511 keV escape peak (1712 keV). There is an underlying, falling continuum due to other flare components as well.

stopping power (high atomic number) and an active Compton shield can keep the diagonal components of this matrix dominant, making interpretation of the spectrum easier. It is not possible to unambiguously invert a nondiagonal instrument response matrix and calculate a unique photon spectrum given the observed count spectrum. The usual practice is to convolve models of the expected spectrum with the response matrix and compare the results to the observed count spectrum.

Monte Carlo tools such as GEANT should be used to model and predict the response matrix for any new design.

## 5 Outlook

Germanium (or, at hard X-ray energies, the other solid state detectors) provides high enough energy resolution for most astrophysical purposes  $> 10$  keV. BGO provides stopping power and large volume up to the mass limit that a launch vehicle can reasonably haul. So the current challenges in detector development are combining high resolution with high volume, and adding fine, 2- or 3-dimensional spatial resolution for Compton telescopes, coded masks, or imagers. Germanium strip detectors provide an appealing compromise of very high spatial and energy resolution with moderate detector volume and stopping power. The key development issues are the difficulty, power and expense of cooling and minimizing the amount of passive material in and around the array, material needed for ther-

mal control as well as mechanical and electrical connections. When very high spatial and spectral resolution are not required, the new lanthanum halide scintillators are becoming a popular option in proposals for space instruments, have spectral resolution better than other scintillators and very good stopping power. They are appealing if their intrinsic background can be tolerated. Recently, high-performance Anger camera prototypes have been developed using SDDs to read out a large scintillator [38; 36]; SDDs have also been coupled to a physically pixelated scintillator [71]. These technologies may provide an interesting alternative to pixelated semiconductors for moderate to high spatial resolution.

Development is also always in progress on other technologies that are promising but still present technical challenges, such as liquid xenon [4; 5], semiconductors such as TlBr [18; 28] and HgI<sub>2</sub> [67], and scintillators such as SrI<sub>2</sub> [70; 26] and BaI<sub>2</sub> [19].

I would like to thank Mark McConnell for very helpful suggestions on the manuscript of this chapter.

## References

1. Agostinelli S et al. (2003) GEANT4 – a simulation toolkit, *Nuc. Inst. Meth. A* 506, 250–303
2. Amman M S and Luke P N (1997) Coplanar-grid detector with single-electrode readout, *Proc. SPIE* 3115, 205–213
3. Amman M and Luke P N (2000) Three-dimensional position sensing and field shaping in orthogonal-strip germanium gamma-ray detectors, *Nuc. Inst. Meth. A* 452, 155–166
4. Aprile E et al. (1998) The electronics read out and data acquisition system for a liquid xenon time projection chamber as a balloon-borne Compton telescope, *Nuc. Inst. Meth.* 412, 425–436
5. Aprile E et al. (1998) Compton imaging of MeV gamma-rays with the Liquid Xenon Gamma-Ray Imaging Telescope (LXeGRIT), *Nuc. Inst. Meth. A* 593, 414–425
6. Atwood W B et al. (2007) Design and initial tests of the Tracker-converter of the Gamma-ray Large Area Space Telescope, *Astroparticle Phys.* 28, 422–434
7. Barthelmy S D et al. (2005) The Burst Alert Telescope (BAT) on the SWIFT Midex Mission, *Space Sci. Rev.* 120, 143–164
8. Berger MJ et al. (1998) XCOM: Photon Cross Sections Database, NIST Standard Reference Database 8 (XGAM) (online)
9. Bicron (Saint Gobain Crystals) (2007) BriLanCe™ 350 (LaCl<sub>3</sub>(Ce)) and BriLanCe™ 380 (LaCl<sub>3</sub>(Ce)) data sheets, <http://www.detectors.saint-gobain.com/>
10. Biggerstaff J A, Becker R L and McEllistrem M T (1961) Charged particle discrimination in a CsI(Tl) detector, *Nuc. Inst. Meth.* 10, 327–332
11. Blosler P F et al. for the MEGA collaboration (2002) The MEGA advanced Compton telescope project, *New Astron. Rev.* 46, 611–616
12. Boggs S et al. (2006) The Advanced Compton Telescope, *Proc. SPIE* 6266:662624-1 – 662624-15
13. Boggs S and Chang Y-H for the NCT collaboration (2007), The Nuclear Compton Telescope (NCT): Scientific goals and expected sensitivity, *Adv. Space Res.* 40, 1281–1287
14. Bolotnikov A E et al. (2001) Development of high spectral resolution CdZnTe pixel detectors for astronomical hard X-ray telescopes, *Nuc. Inst. Meth. A* 458, 585–592
15. Boynton W V et al. (2004) The Mars Odyssey Gamma-Ray Spectrometer Instrument Suite, *Space Sci. Rev.* 110, 37–83
16. Brückner J et al. (1991) Proton-Induced Radiation Damage in Germanium Detectors, *IEEE Trans. Nuc. Sci.* 38, 209–217
17. CERN Application Software Group (1993) Detector Description and Simulation Tool, CERN Program Library Long Writeup W5013
18. Chen H et al. (2008) Characterization of large cadmium zinc telluride crystals grown by traveling heater method, *J. Appl. Phys.* 103, 014903-1 – 014903-5

19. Cherepy N J et al. (2007) Barium iodide single-crystal scintillator detectors, Proc. SPIE Vol. 6706, 670616
20. Dean A J et al. (2003) The Modelling of Background Noise in Astronomical Gamma-Ray Telescopes, Space Sci. Rev. 105, 285–376
21. Diallo N et al. (1996) Impacts of the shield thickness on the induced background, Proc. SPIE 2806, 545–550
22. Fishman G J and Austin R W (1977) Large-area multi-crystal NaI(Tl) detectors for X-ray and gamma-ray astronomy, Nuc. Inst. Meth. 140, 193–196
23. Gehrels N (1992) Instrumental background in gamma-ray spectrometers flown in low Earth orbit, Nuc. Inst. Meth. A 315, 513–528
24. Goldsten J O et al. (2007) The MESSENGER Gamma-Ray and Neutron Spectrometer, Space Sci. Rev. 131, 339–391
25. Harrison F et al. (2005) Development of the HEFT and NuSTAR focusing telescopes, Experimental Astronomy 20, 131–137
26. Hawrami R et al. (2008) SrI<sub>2</sub>: a novel scintillator crystal for nuclear isotope identifiers, Proc. SPIE Vol. 7079, 70790Y
27. Heynderickx D et al. (2004) New radiation environment and effects models in the European Space Agency's Space Environment Information System (SPENVIS), Space Weather, 2, S10S03
28. Hitomi, K et al. (2008) Evaluation of TlBr detectors with Tl electrodes, Proc. SPIE Vol. 7079, 70790J
29. Hurley K (1978) Phosphorescence in CsI Crystals, Astron. Astr. 69, 313–319
30. Jahoda K et al. (2006) Calibration of the Rossi X-Ray Timing Explorer Proportional Counter Array, Astrophys. J. Suppl. 163, 401–423
31. Johnson W N et al. (1993) The Oriented Scintillation Spectrometer Experiment – Instrument description, Astrophys. J. Suppl. 86, 693–712
32. Koenen M et al. (1995) Radiation damage in large-volume n- and p-type high-purity germanium detectors irradiated by 1.5 GeV protons, IEEE Trans. Nuc. Sci. 42, 653–658
33. Knoll G K (2000) Radiation Detection and Measurement, 3rd Edition. John Wiley & Sons, Inc., Hoboken
34. Kurczynski P et al. (1999) Long-term radiation damage to a spaceborne germanium spectrometer, Nuc. Inst. Meth. A 431, 141–147
35. Kurfess J D et al. (2004) An advanced Compton telescope based on thick, position-sensitive solid-state detectors, New Astron. Rev. 48, 293–298
36. Labanti C et al. (2008) Position sensitive x- and gamma-ray scintillator detector for new space telescopes, Proc. SPIE Vol. 7021, 702116
37. Lebrun F et al. (1996) ISGRI: a CdTe array imager for INTEGRAL, Proc. SPIE 2806, 258–268
38. Lechner P et al. (2008) Hard X-ray and gamma-ray imaging and spectroscopy using scintillators coupled to silicon drift detectors, Proc. SPIE Vol. 7021, 702111
39. Lei F, Dean A J, and Hills G L (1997) Compton Polarimetry in gamma-Ray Astronomy, Space Sci. Rev. 82, 309–388
40. Leleux P et al. (2003) Neutron-induced nuclear reactions and degradation in germanium detectors, Astron. Astr. 411, L85–L90
41. Lonjou V et al. (2005) Characterization of the in-flight degradation of the INTEGRAL/SPI detectors, Nuc. Inst. Meth. A, 554, 320–330
42. Luke P N (1988) Low noise germanium radial drift detector, Nuc. Inst. Meth. A 271, 567–570
43. Luke P N (1994) Single-polarity charge sensing in ionization detectors using coplanar electrodes, Appl. Phys. Lett. 65, 2884–2886
44. Mahoney W A et al. (1980) The HEAO-3 gamma-ray spectrometer, Nuc. Inst. Meth. 178, 363–381
45. McGregor D S et al. (1998) Single charge carrier type sensing with a parallel strip pseudo-Frisch-grid CdZnTe semiconductor radiation detector, Appl. Phys. Lett. 72, 792–794
46. Morris D J et al. (1992) Neutron induced background in the COMPTEL detector on the Gamma-Ray Observatory, in The Compton Observatory Science Workshop, NASA, 102–108
47. Natalucci L et al. (2008) CdZnTe detector for hard X-ray and low energy gamma-ray focusing telescope, Proc. SPIE Vol. 7011, 70111S

48. Naya J E et al. (1996) The neutron spectrum inside the shielding of balloon-borne Ge spectrometers, *Nuc. Inst. Meth. A* 368, 832–846
49. Owens A et al. (2007) An assessment of radiation damage in space-based germanium detectors due to solar proton events, *Nuc. Inst. Meth. A*, 583, 285–301
50. ORTEC division of AMETEK, Inc. (2008) LO-AX™ Low-Energy Photon Detector datasheet, <http://www.ortec-online.com/>
51. Pehl R H et al. (1979) Radiation damage resistance of reverse electrode Ge coaxial detectors, *IEEE Trans. Nuc. Sci. NS-26*, 321–323
52. Pirard B et al. (2007) Solar proton damage in high-purity germanium detectors, *Nuc. Inst. Meth. A*, 572, 698–707
53. Raudorf T et al. (1984) Performance of reverse electrode HPGe coaxial detectors after light damage by fast neutrons, *IEEE Trans. Nuc. Sci. NS-31*, 253–257
54. Rehak P et al. (1985) Semiconductor drift chambers for position and energy measurements, *Nuc. Inst. Meth. A* 235, 224–234
55. Richter M and Siffert P (2002), High resolution gamma-ray spectroscopy with CdTe detector systems, *Nuc. Inst. Meth. A* 322, 529–537
56. Rothschild R E et al. (1998) In-flight performance of the high energy X-ray timing experiment on the Rossi X-ray Timing Explorer, *Astrophys. J.* 496, 538–549
57. Sangsingkeow P (1999) Recent developments in HPGe material and detectors for gamma-ray spectroscopy, *Proc. SPIE* 3768, 204–211
58. Schoenfelder V et al. (1993) Instrument description and performance of the Imaging Gamma-Ray Telescope COMPTEL aboard the Compton Gamma-Ray Observatory, *Astrophys. J. Suppl.* 86, 657–692
59. Gamma-ray observations with the Transient Gamma-Ray Spectrometer (TGRS), *Astron. Astr. Suppl.* 120, 653–656
60. Smith D M et al. (1996) All-Sky Search for Transient Sources near 0.5 MeV with the Burst and Transient Source Experiment (BATSE), *Astrophys. J.* 471, 783–795
61. Smith D M et al. (2002) The RHESSI Spectrometer, *Solar Phys.* 210, 33–60
62. Spieler H (2005) *Semiconductor Detector Systems*. Oxford University Press, Oxford New York
63. Takahashi T, Mitsuda K, and Kunieda H (2006) The NeXT mission, *Proc. SPIE* 6266, 62660D-1 – 62660D-12
64. Takahashi T et al. (2007) Hard X-Ray Detector (HXD) on Board Suzaku, *Pub. Ast. Soc. Japan* 59, 35–51
65. Tueller J et al. (2005) InFOCUS hard X-ray imaging telescope, *Exp. Astron.* 20, 121–129
66. Ubertini P et al. (2003) IBIS: The Imager on-board INTEGRAL, *Astron. Astr.* 411, L131–L139
67. van den Berg L et al. (2007) Fabrication and performance of mercuric iodide pixellated detectors, *Proc. SPIE* Vol. 6706, 67060J
68. Vedrenne G et al. (1998) The SPI Spectrometer for the INTEGRAL Mission, *Physica Scripta* T77:35–38
69. Weidenspointner G et al. (2005) MGGPOD: a Monte Carlo Suite for Modeling Instrumental Line and Continuum Backgrounds in Gamma-Ray Astronomy, *Astrophys. J. Suppl.* 156, 69–91
70. Wilson C M et al. (2008) Strontium iodide scintillators for high energy resolution gamma ray spectroscopy, *Proc. SPIE* Vol. 7079, 707917
71. Yamaoka, K et al. (2007) Development of a gamma-ray burst detector based on silicon drift detectors and scintillators, *Proc. SPIE* Vol. 6686, 66860K
72. Zych A D et al. (2006) TIGRE prototype gamma-ray balloon instrument, *Proc. SPIE* 6319, 631919-1 – 631919-10